JOURNAL OF MATERIALS SCIENCE 22 (1987) 3924–3930

X-ray CDF study on the behaviour of the amorphous chain under extension

NOBUO MIYADERA, YUTAKA YOKOYAMA, KEIZO MIYASAKA
Department of Textile and Polymeric Materials, Tokyo Institute of Technology, Ookayama, Meguro-ku, Tokyo 152, Japan

The behaviour of the amorphous chain in vulcanized natural rubber (NR) and styrene-butadiene rubber (SBR) under extension is studied by means of the cylindrical distribution function (CDF) derived from wide angle X-ray scattering (WAXS). In the case of the highly stretched vulcanized NR where the orientation-induced crystallization took place, the observed WAXS intensity was separated into a crystalline peak component and a broad amorphous one from which the CDF was obtained. The CDF calculated from the broad component shows that some of the amorphous segments of the highly stretched vulcanized NR are extended as fully as the crystalline chains and that the fraction of the segments increases with increasing extension. In the case of SBR, such fully stretched segments as in the case of the vulcanized NR show higher degree of an interchain packing order than those in the vulcanized NR.

1. Introduction

It is well recognized that the structure of the amorphous phase in the semi-crystalline polymers plays very important roles to improve the ability of the material; for example, the Young's modulus of semi-crystalline polymers depend much on the degree of amorphous orientation [1, 2]; according to Peterlin [3], the increase in the crystal fraction decreases its free volume of the amorphous phase in some semi-crystalline polymers, resulting in the decrease in the permeabilities of the materials. However, there are very few techniques which can effectively characterize the structure of properties of the amorphous phase, contrary to the many techniques applicable to the crystalline phase.

Some workers have applied the cylindrical distribution function (CDF) technique to the investigation of non-crystalline polymers. Norman [4] first calculated the CDF of cellulose, and recently Mitchell *et al.* [5] obtained CDF's for some non-crystalline polymers oriented by extension. The CDF is a Fourier transform of the X-ray scattering intensity from the sample which has a cylindrically symmetrical structure, and gives informations about the length and the direction of vectors relating pairs of atoms or electrons. It is the autoconvolution of the structure. Moreover, the CDF is calculated from the experimental scattering intensity without any assumptions for the structure. As for the orientation informations, all orders of Legendre polynomials are involved in CDF, in contrast to other techniques which relate only to limited orders of moments of the polynomials; birefringence and dichroism are determined by the second order moment, while Raman and fluorescence are determined by the second and the fourth order moments.

In an earlier work [6], we measured the change in the CDF's for the amorphous phase of Nylon-6 fibres as a function of the stretching stresses, to determine how the amorphous chains in a fibre behave under extension. It was the first case in which the CDF technique was applied to the study on the structure of the amorphous phase in the semicrystalline polymer.

In this work, we measured the wide angle X-ray scattering intensity of vulcanized natural rubber (NR) and styrene-butadiene rubber (SBR) as a function of extension ratio, to calculate the CDF. Our interest is to know how the chains behave under extension from the changes of CDF. It should be remarked that an orientation-induced crystallization occurs under high extension of NR.

2. Experimental procedure

Vulcanized NR and SBR films 1 mm thick were prepared according to the recipes shown in Table I and II, respectively. Strips 25 mm wide and 10 cm long were cut from the films and stretched to a given extension ratio at room temperature in an Instron type extensometer. After being held at the extension more than 1 h, the extended specimen was fixed to the sample holder for X-ray measurement. Nickel filtered Cu$K\alpha$ ray from Rigakudenki Ru-200 driven at 50 kV and 200 mA was used in pinhole collimation systems for the incident and the scattered rays. The scattering intensity was measured by a scintillation counter as a function of both the scattering angle 2θ from 6 to 120° and the azimuthal angle α measured from the direction of stretching at intervals of 9°. The scanning speed was 1 deg min^{-1} and time constant was 1 sec.

The orientation-induced crystallization took place during extension of vulcanized NR. In order to estimate the intensity of the amorphous phase the structure of which we are interested in, the observed intensity was separated into a peak component and a broad one, under an assumption that the crystalline intensity

0022–2461/87 $03.00 + .12

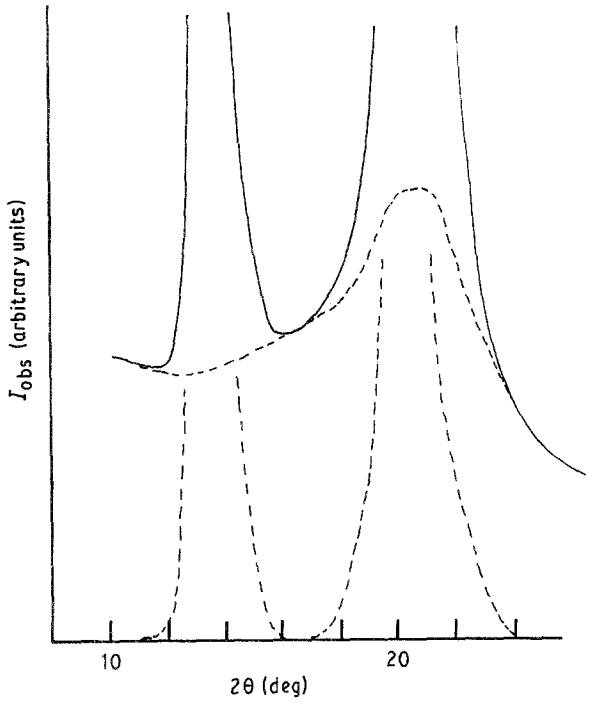

Figure 1 An equatorial X-ray scattering intensity from the vulcanized NR under extension of $\lambda = 6$: (——) the observed intensity; (– – –) the separated amorphous and crystalline intensities.

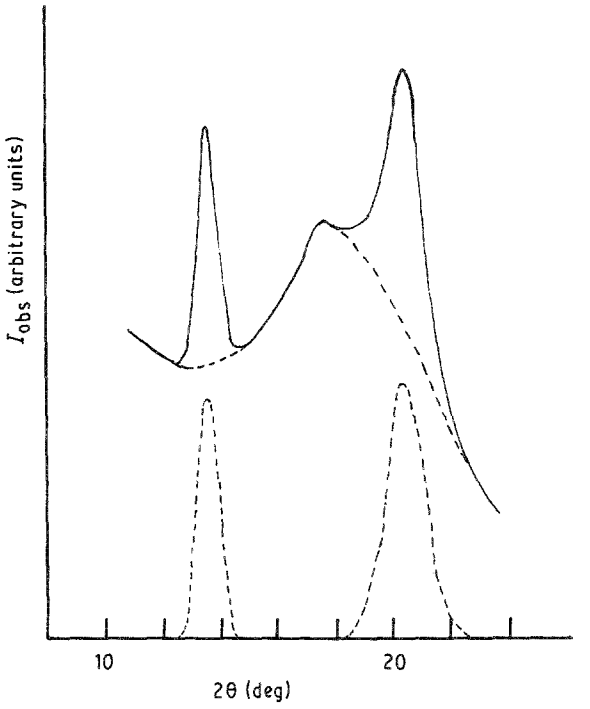

Figure 2 An equatorial X-ray scattering intensity from the vulcanized NR under extension of $\lambda = 4$: (——) the observed intensity; (– – –) the separated amorphous and crystalline intensities.

was involved only in the peak component and the amorphous one was in the broad one.

Fig. 1 shows the scattering intensity at $\alpha = \pi/2$ from the vulcanized NR under extension of $\lambda = 6$. This is an example of the most difficult cases in the separation of the most difficult cases in the separation of the crystalline and the amorphous intensity, because the (120) diffraction peak is very strong and the amorphous broad peak is overlaid by its tail. However, the separation was easy under lesser extensions, as shown in Fig. 2 for $\lambda = 4$ at $\alpha = \pi/2$. The degree of crystal orientation was very high in the case of orientation-induced crystallization, and therefore a crystalline peak which appeared at a given azimuthal angle no longer appeared at the next azimuthal angle which was 9° away from that. On the other hand, the amorphous intensity had less azimuthal angle dependency than that of crystalline diffraction. In this case, when the separation of the amorphous intensity component at a given azimuthal angle α was carried out, the intensity curves at the angles $\alpha \pm 9°$ was taken into consideration. It made the separation easier and more accurate.

The profile of crystalline peak which depends on the size and the regularity of the crystal lattice is expected to be symmetrical. This criterion of the symmetry of the profile helped us to separate the amorphous scattering, together with reference to the intensity data under lower extension ratio and at the neighbouring azimuth under the same extension. The diffraction peaks from ZnO crystals were also removed in the same way as that for the crystalline phase.

The amorphous intensity data thus evaluated were fed to a computer with a digitizer, and then corrected for air scattering, absorption and polarization. The corrected data $I_{corr}(s, \alpha)$ was then normalized by the factor K which was calculated by Equation 1 from I_{ind} and I_{av}, assuming that the scattering intensity at $2\theta = 120°$ was contributed only by its independent scattering of atoms.

$$K = I_{ind}(2\theta = 120°)/I_{av}(2\theta = 120°) \quad (1)$$

where K is the normalization factor, and $I_{ind}(2\theta = 120°)$ is the value at $2\theta = 120°$ of $I_{ind}(s)$ which is calculated by Equation 2

$$I_{ind} = \sum_{j=1}^{n} C_j(f_j(s)^2 + I_{j,inc}(s)) \quad (2)$$

where C_j is the number fraction of jth atom, $f_j(s)$ and $I_{j,inc}(s)$ are the atomic structure factor and the

TABLE I A recipe for the vulcanized NR

Material	Composition
NR	100 (phr)
ZnO	5
stearic acid	3
antioxidant	1
vulcanization accelerator	1
sulphur	1.8
condition of vulcanization	148° C, 20 min.

TABLE II A recipe for SBR

Material	Composition
SBR(1502)	100 (phr)
carbon black(HAF-HS)	50
ZnO	5
stearic acid	3
antioxidant	1
vulcanization accelerator	1
sulphur	1.8
condition of vulcanization	148° C, 25 min.

incoherent scattering, respectively. $I_{av}(2\theta = 120°)$ in Equation 1 is the intensity at $2\theta = 120°$ averaged over all azimuth by Equation 3.

$$I_{av} = \int_0^{\pi/2} I_{corr}(120°, \alpha) \sin \alpha d\alpha \quad (3)$$

where $I_{corr}(120°, \alpha)$ is the corrected intensity at $2\theta = 120°$ and a given azimuthal angle α.

The independent scattering intensity was then subtracted from the normalized, corrected intensity $KI_{corr}(s, \alpha)$ to obtain a reduced intensity $i(s, \alpha)$.

$$i(s, \alpha) = KI_{corr}(s, \alpha) - I_{ind}(s) \quad (4)$$

For the atomic structure factor $f_j(s)$ and incoherent scattering $I_{j,inc}(s)$, the functions proposed by J. T. Waber [7] (Equation 5) and F. Hajdu [8] (Equation 6) were used, respectively.

$$f_j(s) = \sum_{i=1}^{n} a_{j,i} \exp(-b_{j,i}s^2) + C_j \quad (5)$$

where $a_{j,i}$, $b_{j,i}$ and C_j are the parameters given in the article [7].

$$I_{j,inc}(s) = (Z_j - f_j(s)^2/Z_j)(1 - M_j(\exp(-k_j s) - \exp(-l_j s))) \quad (6)$$

where Z_j is the atomic number of jth atom, and M_j, k_j and l_j are the parameters given in the article [8].

In this work, an electronic CDF was obtained, for the sharpening function $(\Sigma\ C_j f_j(s))^2$ was not used, where C_j and $f_j(s)$ are the number fraction and the structure factor of jth atom, respectively. We were concerned that the modification by the sharpening function might exaggerate any termination errors. To obtain an atomic CDF, Equation 4 was divided by the sharpening function and usually multiplied by the damping factor $\exp(-as^2)$ to diminish the termination error [9]. But in this work, the damping factor was not used, because we were concerned about possible effect of distortion of the function. There was, however, little difference between our method and the traditional one in which both the sharpening function and the damping factor were used, because the two functions had nearly the same shapes [10]; one of them was in the denominator and the other was in the numerator.

The transformation of $i(s, \alpha)$ was performed with Equations 7 to 10.

$$i(s, \alpha) = \sum_{n=0}^{\infty} i_{2n}(s) P_{2n}(\cos \alpha) \quad (7)$$

where P_{2n} is the $2n$th order of Legendre polynomials.

$$i_{2n}(s) = (4n + 1) \int_0^{\pi/2} i(s, \alpha) P_{2n}(\cos \alpha) \sin \alpha d\alpha \quad (8)$$

$$W_{2n}(r) = (-1)^n (2r/\pi) \int_0^{\infty} s^2 i_{2n}(s) j_{2n}(rs)\, ds \quad (9)$$

where j_{2n} is $2n$th order of spherical Bessel functions.

$$W(r, \alpha) = \sum_{n=0}^{\infty} W_{2n}(r) P_{2n}(\cos \alpha) \quad (10)$$

The Legendre polynomials and spherical Bessel functions were prepared up to $2n = 12$. In this work, a fairly good convergence was achieved for the expansion in a series of Legendre polynomials. Even for the sample with the highest degree of orientation, the amplitude of the 12th order $i_{12}(s)$ was about 5% of that of the 0th order $i_0(s)$.

The integration in Equation 9 was terminated at the s corresponding to $2\theta = 120°$ where the termination error for all components was minimized by a sampled transform technique proposed by R. Lovell *et al.* [10]. In this work, the final results of the CDF calculation are shown by $rW(r, \alpha)$ defined by Equation 11.

$$rW(r, \alpha) = 4\pi r^2(\varrho(r, \alpha) - \varrho_0) \quad (11)$$

where $\varrho(r, \alpha)$ is the auto correlation function of the electron density and ϱ_0 is the average electron density. The use of many subroutines for the computer program made the calculation much faster than in the previous report [6]. The contour maps of CDF's were figured with Mori's program [11].

3. Results and discussion

Figs. 3–6 show the contour maps of CDF derived from the amorphous intensity for the stretched vulcanized NR. The ordinate is parallel to the stretching direction, which is identical to the symmetry axis of cylindrical distribution of electron density, and the abscissa is normal to the direction. Broken thin contours are negative, and heavy full contours are zero, where the electron density is equal to the average density ϱ_0.

Fig. 3 shows CDF for unstretched vulcanized NR at room temperature. The concentric contours indicate that the amorphous chain does not show any orientation. The CDF's at various extension ratios are shown in Figs. 4–6. There appear several "mountains" and "valleys" under extension, which are due to both the extension and the preferable orientation of amorphous chains. The contours forming concentric circles decrease in number with increasing extension ratio, indicating the increase in the orientation of amorphous chains.

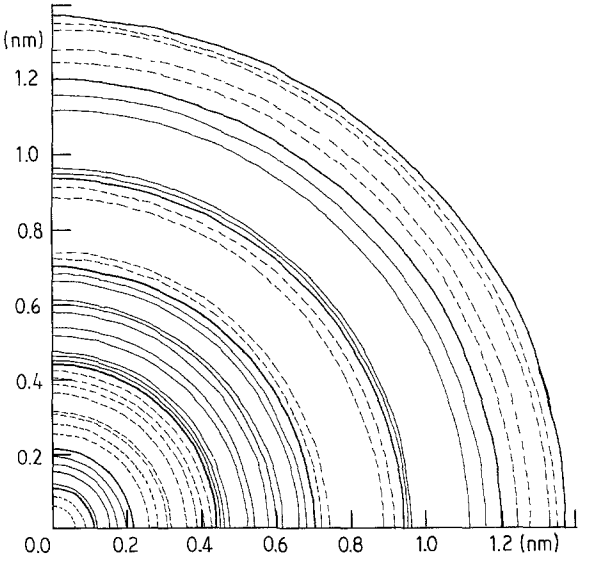

Figure 3 A contour map of CDF for the unstretched vulcanized NR: (——) positive; (– – –) negative; (——) zero.

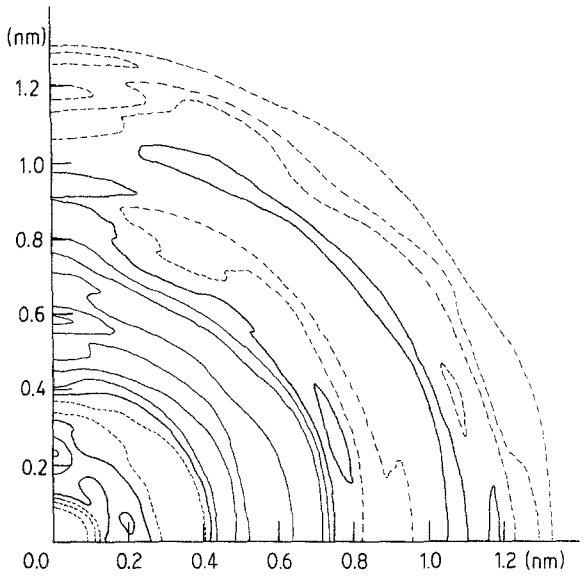

Figure 4 A contour map of CDF for the amorphous of the vulcanized NR under extension of $\lambda = 3$: (——) positive; (– – –) negative; (——) zero.

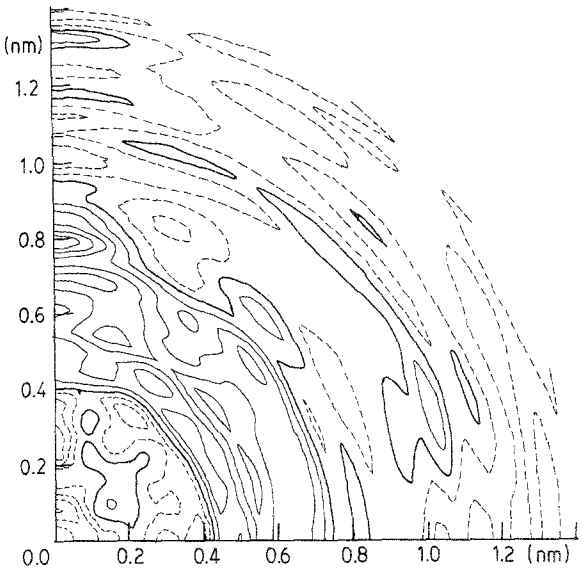

Figure 6 A contour map of CDF for the amorphous of the vulcanized NR under extension of $\lambda = 6$: (——) positive; (– – –) negative; (——) zero.

In Fig. 6 the CDF for the highest oriented sample has the first equatorial peak near 0.6 nm which is attributable to the interchain structure. Thus the broad peak at 0.6 nm in the DRDF of unstretched vulcanized NR which have been reported previously by many workers [12] is proved to be due to the interchain distance.

On the other hand, there are interchain peaks near the meridian from which we are able to get the information about chain conformation. Particularly, we wish to focus attention on the meridional peak at 0.8 nm which appears only under high extensions (see Figs 5 and 6). It is interesting to remark that the amorphous chain segments having a periodicity of 0.8 nm in the stretching direction increase in number with extension. This 0.8 nm in a chain direction is in accord with the C-axis spacing of the NR crystal. Thus we suppose the strong meridional peak at 0.8 nm suggests that there is a significant number of highly stretched amorphous chains which have nearly the same conformation as that in crystals.

The atomic auto correlation function $\varrho(r, \alpha)$ calculated for a single crystal chain of NR is shown in Fig. 7. In this calculation, we adopted the crystalline structure model obtained by Bunn [13].

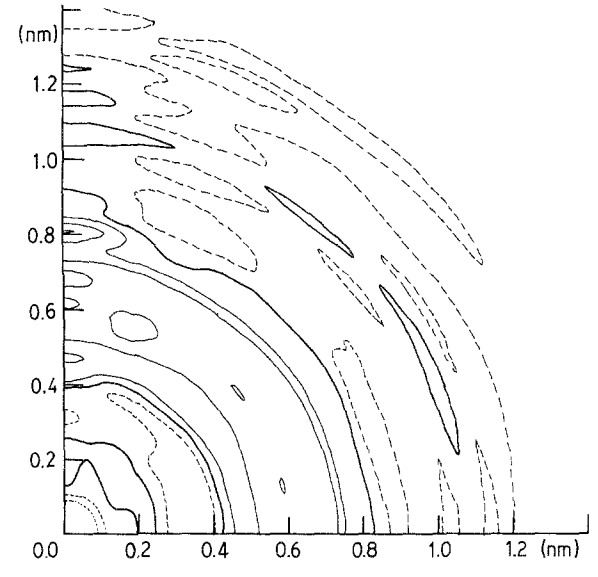

Figure 5 A contour map of CDF for the amorphous of the vulcanized NR under extension of $\lambda = 4$: (——) positive; (– – –) negative; (——) zero.

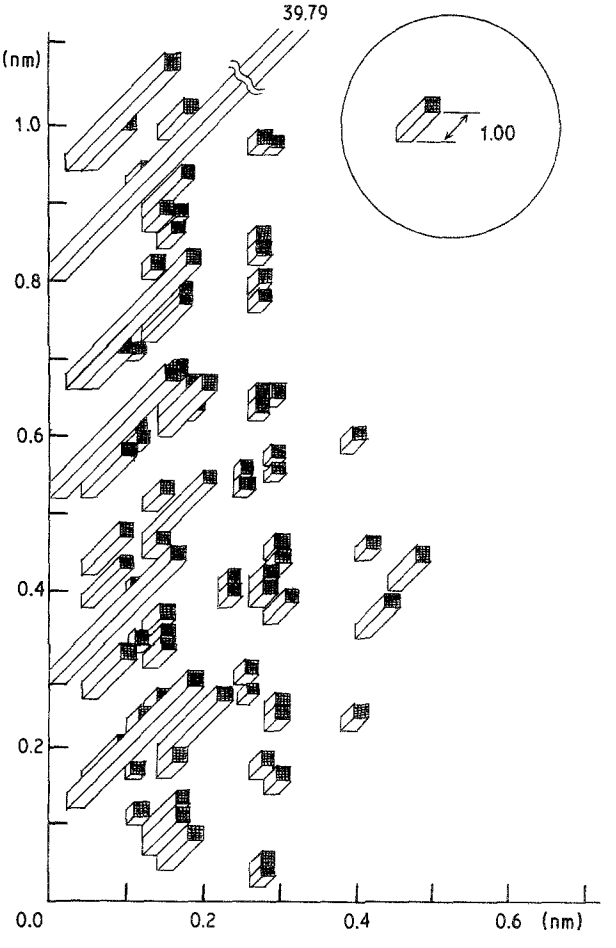

Figure 7 The atomic ratio correlation function calculated for a single crystal chain of NR. The square pillar in a circle represents a unit height.

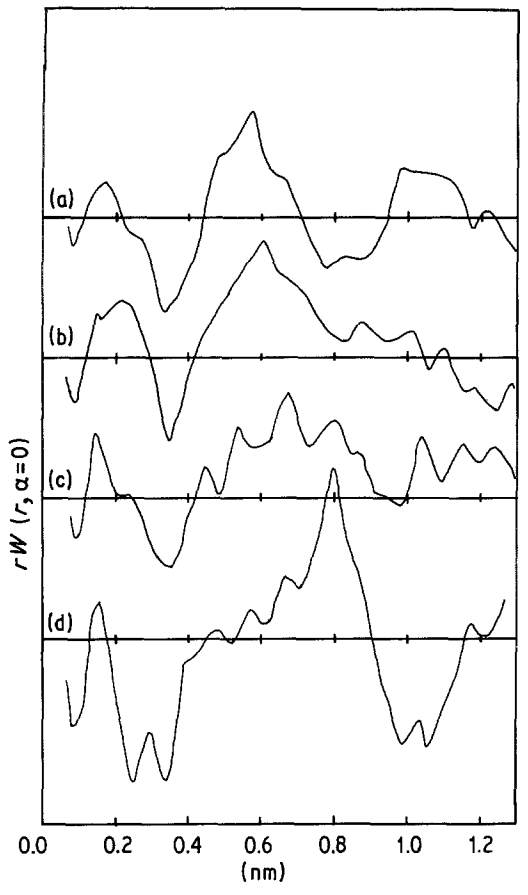

Figure 8 The meridional CDF intensities for the vulcanized NR under various extensions as a function of r: (a) $\lambda = 1$; (b) $\lambda = 3$; (c) $\lambda = 4$; (d) $\lambda = 6$.

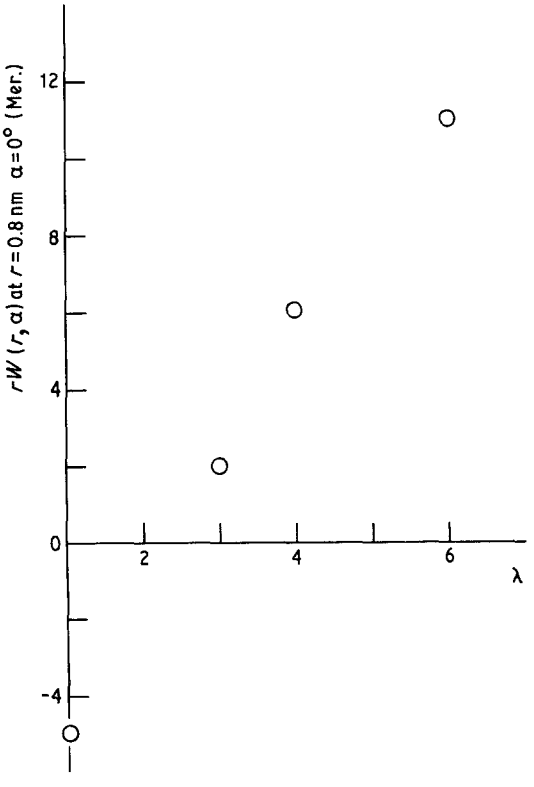

Figure 9 The intensity of CDF meridional peak at 0.8 nm as a function of an extension ratio (see equation 11).

Since the chain conformation in the crystal is definite, $\varrho(r, \alpha)$ is the point function. We calculated this function with the resolution of 0.02 nm, then we represented it with a bird's eye view of the square pillars, each base area of which is 0.0004 nm^2 and each height of which is proportional to the sum of $\varrho(r, \alpha)$ in its base area. Comparing Fig. 7 with Fig. 6, some features of Fig. 7 appear in Fig. 6. The meridional peaks at 0.15 nm, 0.3 nm (this meridional peak at 0.3 nm is maximum in negative region as shown in Fig. 8d), 0.52 nm and 0.8 nm in Fig. 6 correspond to those in Fig. 7. The peaks at 0.12 nm, 0.17 nm and 0.2 nm in the abscissa and 0.08 nm, 0.18 nm, and 0.6 nm in the ordinate, respectively are also seen both in Fig. 6 and in Fig. 7.

Fig. 9 shows the meridional intensity at 0.8 nm as a function of the extension ratio, indicating that the intensity is getting stronger with increasing extension ratio. The intensity reflects the number of pairs of atoms 0.8 nm away from each other and parallel to the stretched direction. As shown in Fig. 8, the peak at 0.8 nm appears only under high extension ($\lambda \geqslant 4$), and is getting sharper and stronger with increasing extension ratio. Usual amorphous polymers does not have any sharp peaks at such a long distance as 0.8 nm. These facts suggest that the peak at 0.8 nm does not attribute to the interchain pairs of atoms, but to the intrachain pairs of atoms. Thus the amorphous chains which have the same conformation as that in crystals increase in number with increasing extension ratio. Furthermore, as shown in Fig. 8, the meridional peaks are getting sharper with increasing extension ratio. Thus under high extension, the fluctuation in the conformation of amorphous chains becomes smaller, approaching to that of crystalline chains.

Although highly stretched amorphous chains and crystalline chains have almost the same conformation, they must have different modes of interchain alignment which is reflected on the nature of CDF on the equator. The first equatorial peak in CDF for highly stretched vulcanized NR is at about 0.6 nm and the second relatively small one is at about 1.2 nm. Those equatorial peaks are as broad as that for monoatomic liquids [14], suggesting that the amorphous chains in highly stretched vulcanized NR have much less interchain regularity compared with crystalline chains, even if the former has the same conformation as the latter.

Figs 10–12 show CDF's for SBR of $\lambda = 1$, $\lambda = 3$ and $\lambda = 4$, respectively. In contrast to NR, SBR does not crystallize by extension. In Fig. 12, the chain orientation is better than that in Fig. 11. It is interesting to remark that the CDF for SBR has much sharper equatorial peaks compared with these of vulcanized NR. In the case of SBR, the first relatively sharp equatorial peak at 0.5 nm is followed by the second one at 1.0 nm which is still discrete, while in the case of NR the equatorial peaks at 0.6 nm and 1.2 nm are very broad and weak. At the same time it should be noted that the 0.5 nm peak appears also on the meridian in Fig. 12, showing the maximum intensity stronger than that on the equator. This meridional 0.5 nm peak together with 0.25 nm one is considered due to the

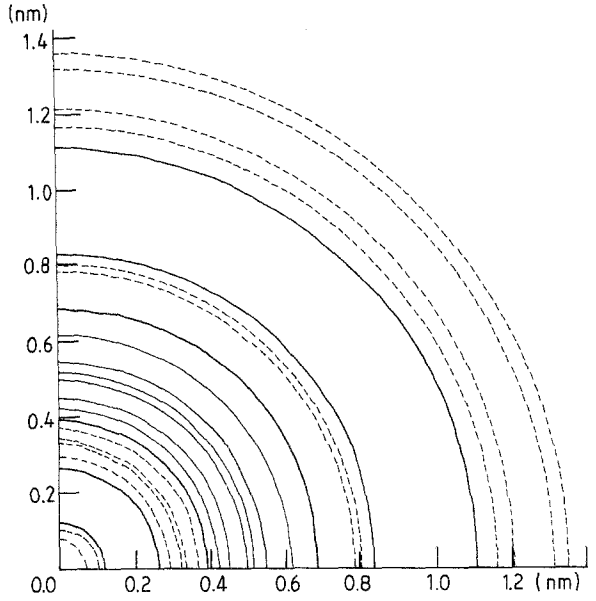

Figure 10 A contour map of CDF for the unstretched SBR: (——) positive; (– – –) negative; (——) zero.

intrachain electron pairs, and therefore the appearance of these peaks indicates the origination of highly extended and oriented segments. These features of CDF for SBR under high extension suggest that SBR chains are stretched and oriented in the direction of extension so that they can be packed side by side, as is the case of liquid crystals. This feature of SBR corresponds to our previous result [15] that under uniaxial extension an equatorial peak appears at $2\theta = 20°$ for Cu$K\alpha$ ray on the X-ray scattering curve. The peak grew stronger and shifted the maximum to larger scattering angle with increasing extension ratio, indicating the increases in the packing density and in the fraction of the oriented and well packed segments.

It may be interesting to point out that some of the amorphous segments can be extended almost as fully as the crystalline chains. In the case of crystalline polymers below the melting point, the highly extended

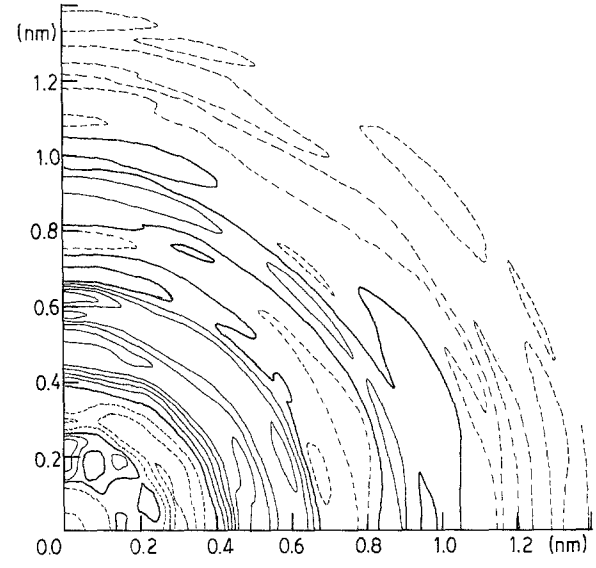

Figure 11 A contour map of CDF for the SBR under extension of $\lambda = 3$: (——) positive; (– – –) negative; (——) zero.

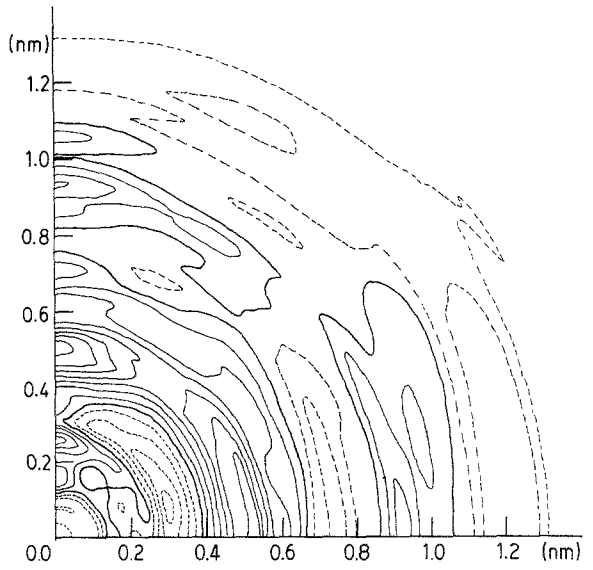

Figure 12 A contour map of CDF for the SBR under extension of $\lambda = 4$: (——) positive; (– – –) negative; (——) zero.

segments may contribute to the nucleus-formation to promote the crystallization. The very high degree of orientation of the segments necessarily causes highly oriented crystals, as is well known. In the case of non-crystalline polymers, the extended segments are forced to be packed side by side under extension force, forming a temporary structure like a nematic liquid crystal.

Conclusions

We applied the CDF technique to investigate a behaviour of the amorphous chains under extension in vulcanized NR and SBR. Under high extension, some of the amorphous segments were almost fully stretched and the fraction of the segments increased with increasing extension. In the case of vulcanized NR, such fully stretched segments seem to be possible only with coexistence of the crystals formed by extension. In the case of SBR, such fully stretched segments are packed side by side.

Acknowledgement

This work was supported by a Grant-in-Aid from the Ministry of Education in Japan.

References

1. J. SHIMIZU, N. OKUI and T. KIKUTANI, *Sen-i Gakkaishi* **37** (1981) T-135.
2. S. HOSHINO, J. POWERS, D. G. LEGRAND, H. KAWAI and R. S. STEIN, *J. Polym. Sci.* **58** (1962) 185.
3. A. PETERLIN and F. L. McCRACKIN, *J. Polym. Sci., Phys. Edn.* **19** (1981) 1003.
4. N. NORMAN, *Acta Cryst.* **7** (1954) 462.
5. G. R. MITCHELL and R. LOVELL, *Acta Crystallogr.* **A37** (1981) 189.
6. K. OSAWA, K. MIYASAKA and K. ISHIKAWA, *Fiber Science and Technology Japan,* Preprints (1983) p. 63.
7. D. T. CROMER and J. T. WABER, *Acta Crystallogr.* **18** (1965) 104.
8. F. HAJDU, *Acta Crystallogr.* **A27** (1971) 73.
9. H. P. KLUG and L. E. ALEXANDER, in "X-ray Diffraction Procedures" (John Wiley and Sons, New York, 1974) p. 823.
10. R. LOVELL, G. R. MITCHELL and A. H. WINDLE, *Acta Crystallogr.* **A35** (1979) 598.

11. M. MORI, in "Kyokusen to Kyokumen (A Curved Line and A Curved Surface)" (Kyouikushuppan, Tokyo, Japan, 1974) p. 70.
12. C. S. WANG and G. S. Y. YEH, *J. Macromol. Sci.-Phys.* **B15** (1978) 107.
13. C. W. BUNN, *Proc. Roy. Soc.* **A180** (1942) 40.
14. P. A. EGELSTAFF, in "An Introduction to the Liquid State" (Academic Press, London and New York, 1967); (Yoshioka Shoten, Kyoto, Japan, 1971) p. 18.
15. R. OONO, K. MIYASAKA and K. ISHIKAWA, *Kobunshi-Kagaku* **29** (1972) 327.

Received 27 May 1986
and accepted 20 March 1987